Advanced deep flux weakening operation control strategies for IPMSM

Pham Quoc Khanh[1], Ho Pham Huy Anh[2]
[1]Faculty of Electricity Technology (FEE), Industrial University of Ho Chi Minh City (IUH), Vietnam
[2]Faculty of Electrical and Electronics Engineering (FEEE), Ho Chi Minh City University of Technology (HCMUT),
VNU-HCM, Ho Chi Minh City, Vietnam

ABSTRACT

This paper proposes an advanced flux-weakening control method to enlarge the speed range of interior permanent magnet synchronous motor (IPMSM). In the deep flux weakening (FW) region, the flux linkage decreases as the motor speed increases, increasing instability. Classic control methods will be unstable when operating in this area when changing load torque or reference speed is required. The paper proposes a hybrid control method to eliminate instability caused by voltage limit violation and improve the reference velocity-tracking efficiency when combining two classic control methods. Besides, the effective zone of IPMSM in the FW is analyzed and applied to enhance stability and efficiency following reference velocity. Simulation results demonstrate the strength and effectiveness of the proposed method.

This is an open access article under the [CC BY-SA](#) license.

Corresponding Author:

Ho Pham Huy Anh
Faculty of Electrical and Electronics Engineering (FEEE)
Ho Chi Minh City University of Technology (HCMUT), VNU-HCM
268 Ly Thuong Kiet, 10th District, Ho Chi Minh City, Vietnam
Email: hphanh@hcmut.edu.vn

1. INTRODUCTION

Nowadays, electric vehicles (EV) are widely used to improve efficiency and reduce greenhouse gas emissions by internal combustion engines [1]. There are many EV manufacturers involved in the production of electric vehicles, such as Benz, Tesla, Honda, and Toyota [2]. Electric vehicle systems are more efficient and have a more comprehensive range of speeds than vehicles using internal combustion engines. With permanent magnet synchronous motor (PMSM) actuators, operating at sub-rated speeds is the central area of activity, and many studies proposed some approaches to improve operating efficiency [3]-[8]. However, under certain operating conditions in some electric vehicles, it is also required to accelerate the engine to above-rated speeds. Therefore, running in the magnetic field is one criterion for evaluating current electric cars [2]. There are two main types of PMSM mentioned in velocity control: IPMSM and SPMSM. SPMSM is constructed of magnets that are mounted on or inserted on the rotor. The IPMSM has a structure of magnets arranged inside the hollow cavities of the rotor. In applications with high rotor speeds, the centrifugal force will be so great that IPMSM often appears to be more efficient mechanically than SPMSM [9]. In this paper, IPMSM is used to study the PMSM velocity control problem in the DFW region.

There are three main parts of the operating speed range of PMSM: Constant torque, constant power, and decreasing power region. The torque always ensured that it does not exceed the manufacturer's value in the area below the base speed. When the rotor speed exceeds the motor rated speed, the machine will change

from constant torque to constant power. PMSM power was kept so as not to exceed its rated capacity in the region above base speed. However, the speeding capability of PMSM is not infinite. When the motor speed exceeds a certain threshold, its power is decreasing. Figure 1 shows the operating speed range of PMSM.
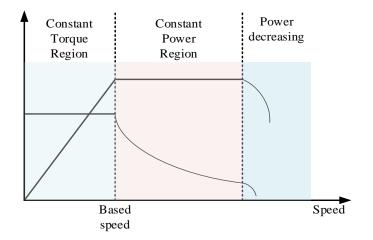

Figure 1. The operating speed range of PMSM

In the constant-torque region, different algorithms aim to maximize the torque on the stator current (MTPA). In this functional area, the motor speed changed by changing the q-axis current accordingly. The d-axis current changed to the operating point is on the MTPA curve, as shown in Figure 2. They lead to the linkage flux value between the rotor and the stator almost constant. Back electromotive force (BEMF) increases proportionally to the motor speed. The constant torque region ends when the PMSM velocity reaches the rated speed, at which time the BEMF also reaches the limit value that can be supplied by the inverter.
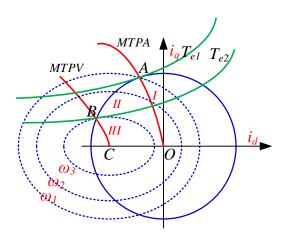

Figure 2. PMSM operating velocity range in the *id-iq* plane

When the motor operates at a constant power area with a rotor speed higher than the rated rotor speed, the Flux linkage must be reduced so that the BEMF does not exceed the limit value at the inverter output. The rotor flux is made of permanent magnets not to be changed over a wide range, so the stator's magnetic field is used to weaken the permanent magnet flux associated with the stator coil. Increasing the d-axis current component in the negative direction leads to reduce flux linkage. The d-axis current will change until the BEMF on the stator drops below the limit voltage. The q-axis current needs to change following the d-axis current. The control method for increasing PMSM motor speed above the rated speed by reducing the flux linkage is called the flux-weakening control.

In technological development, the demand for motors capable of operating at a wide range of speeds has also increased. Jahns proposed operation in the FW region for IPMSM in the study [10], and this is the beginning of research on constant power region in PMSM speed control. There are two ways to increase the speed range of a PMSM; one is to change the rotor structure so that the motor can increase the operating range by increasing the motor rated speed. The second way is to apply the PMSM control algorithm in FW to put the motor at speed greater than the rated speed. The method of structural change to improve the performance of PMSM has been proposed in the studies [11], [12]. The second direction of research is the impact on control software, proposed FW algorithms to improve the speed's range. Based on the classification of the study [13], there are four main methods in PMSM velocity regulation in FW area: TFLUT test [14]-[16], direct current calculation (DCC) [17]-[19], vector current control (VCC) [20]-[22] và flux vector control (FVC) [23]-[25]. Bolognani *et al.* [26] gave some comparisons between these control algorithms. The comparison is shown in Table 1.

Table 1. Comparison of efficiency between FW methods

Approach	VCC	DCC	FVC	LUT
Implementation	Simple implementation	simple implementation	simple implementation	complex implementation
Stability in the FW region	Performance is reduced between different work areas under the influence of controller parameters	Stable operation	Stable operation	Stable operation when strong magnetic saturation effects
Acceleration state	Automatic management of transitions between MTPA and flux-weakening control	transitions between MTPA and flux-weakening control is not convenient when the working point is always outside the current limit circle	transitions between MTPA and flux-weakening control is not convenient when the working point is always outside the current limit circle	The roaming is quite convenient based on the lookup table.

The reduced electromagnetic force in the DFW region makes the electromechanical link unstable. Steady speed control in this area is often more difficult [27]. The inverter's voltage amplitude in the FW region is also pushed up to the rated value, making the current control more restrictive than the constant torque region. A slight change in the working conditions of the IPMSM can also cause work point instability. With changing the speed of electric trams, large fluctuations in speed change are the main disadvantages of PMSM control in the FW region.

The paper proposed a hybrid speed control algorithm combining two-speed control PMSM in FW, namely VCC and FVC. The switching between these 2 techniques is done using rotor speed and reference current value. The proposed hybrid control method is novel. It uses the FVC method's advantages in the internal area of the FW to eliminate the inverter limit voltage violation and uses the benefits of the VCC method to shorten the time to accelerate. Simulation results are recorded through simulation modeling using MATLAB/Simulink software and are presented in detail afterwards.

The remainder is structured with the part 2 presents the math model and workspaces of an IPMSM. Part 3 presents a hybrid control method for PMSM in the proposed FW region. Part 4 shows the results obtained after the simulation modeling for the proposed algorithm and the DCC and VCC algorithm used in the comparison. Part 5 is the conclusion.

2. THE MATH MODEL AND THE CONTROL CURVES OF IPMSM
2.1. IPMSM model and voltage-current limits
According to [28], Basic electrical equations of IPMSM in the dq coordinate system are presented in the (1), (2), (3):

$$v_d = R_s.i_d + L_d.di_d / dt - \omega_e L_q i_q \tag{1}$$

$$v_q = R_s.i_q + L_q di_q / dt + \omega_e L_d i_d + \omega_e \lambda_{pm} \tag{2}$$

$$T_e = 1.5P\left(\lambda_{pm}i_q + \left(L_d - L_q\right).i_q i_d\right) \tag{3}$$

where

L_d and L_q is the d-axis and q-axis inductance, respectively.

v_d and v_q is the d-axis and q-axis voltage, respectively.

i_d and i_q is the d-axis and q-axis current, respectively.

λ_{pm} is the amplitude of flux linkage due to the permanent magnet and R_s is the stator coil's resistance.

According to [3], (4) determined The acceleration as:

$$\frac{d\omega_m}{dt} = \frac{1}{J}\left(T_e - T_L - F\omega_m\right) \tag{4}$$

In which:

J : Inertial value of PMSM-load linked referred to PMSM shaft.

F : Jointed viscous factor of loaded PMSM.

θ : Rotating angle location.

T_e : Electromagnetic Torque.

T_L : Load torque.

ω_m : Rotating angle speed

PMSM current and voltage are bounded by its nominal magnitudes in which voltage boundary depends on PMSM isolation capability with maximum voltage magnitude that the inverter could provide. Manufacturer supplies the current limit. It is related to heat dissipation for the active power losses generated inside the motor. The (5) and (6) describe the limitations of voltage and current, respectively:

$$v_d^2 + v_q^2 = v_s^2 \le v_{s,\max}^2 \tag{5}$$

$$i_d^2 + i_q^2 = i_s^2 \le i_{s,\max}^2 \tag{6}$$

where v_s is the vector amplitude of the inverter voltage, $v_{s,max}$ is the maximum voltage amplitude of the inverter, i_s is the vector amplitude of the current flows into the stator coil, and $i_{s,\max}$ is the rated value of the current injected into the stator coil.

In case motor velocity is greater than motor nominal value, the BEMF appearing at stator winding under the influence of the variable flux when the rotor is spinning will be much greater than the voltage drop the winding caused by the stator resistance. The value of the voltage drop on the stator windings can be ignored at this time. On the other hand, the *dq* axis currents in the steady-state are considered constant, which allows the derivative of the component currents to be eliminated $(di_d / dt = 0; di_q / dt = 0)$. At this point, the stator voltage (1) and (2) rewritten as (7), (8):

$$v_d = -\omega_e L_q i_q \tag{7}$$

$$v_q = \omega_e L_d i_d + \omega_e \lambda_{pm} \tag{8}$$

The relationship between rotor speed and component currents is built through (9) by substitute (7) (8) into (5).

$$\left(L_q i_q\right)^2 + \left(L_d i_d + \lambda_{pm}\right)^2 \le \frac{v_{s,\max}^2}{\omega_e^2} \tag{9}$$

Based on the (6), the working point of the IPMSM must be inside a solid blue circle centered on O and the radius OA as shown in Figure 2 While working within this point, current flows in the coil will not exceed the rated current, thereby ensuring the motor does not overheat. The dashed blue circles form the relationship between the stator current and the inverter's output voltage. Based on the (9), to ensure that the stator winding voltage does not exceed the maximum permissible value of the inverter, the working point must be in this ellipse. Thus, when the IPMSM motor operates at a constant power area, in addition to the standard current limit, the current is also bound by the limitation of voltage.

2.2. Optimal working areas of PMSM

MTPA curve: When operating at a low speed below the rated speed, the control goal now is to minimize the copper loss that causes current to flow in the stator coil. With the same electromagnetic torque required, the stator component currents are calibrated so that this current amplitude is minimal. According to [18], the dq-axis current calculated from the stator current amplitude is presented in (10). The OA curve in Figure 2 shows the working point orbits in the constant moment region.

$$i_{d,mpta} = \frac{\lambda_{pm} - \sqrt{\lambda_{pm}^2 + 8\left(L_d - L_q\right)^2 . i_s^2}}{4\left(L_q - L_d\right)}$$

$$i_{q,mpta} = \sqrt{i_s^2 - i_{d,mpta}^2}$$

$$(10)$$

The maximum current (MC) curve: The BEMF on the stator winding will exceed the inverter's limiting voltage when the rotor speed exceeds the rated speed value. At this time, the d-axis component current increases in the negative direction so that the stator voltage drops and avoids overvoltage. The q-axis component current will also decrease accordingly so that the current amplitude does not exceed the rated current. Thus, for the obtained electric moment to be maximum during acceleration, the stator current amplitude must be set to equal the rated current during acceleration. The d-axis current will be increased by increasing the current vector angle to decrease the stator voltage. The q-axis current will be recalibrated to the stator current vector, as shown in (11) where β is the current vector angle.

$$i_d = i_{s,max} . \cos \beta$$

$$i_q = i_{s,max} . \sin \beta$$

$$(11)$$

Maximum torque per volt: The contact between the constant moment curve and the voltage limit ellipse is where the lowest voltage is found in the points on the constant torque curve. This set of contacts will record the accumulation of the points with the highest torque on the same stator voltage value and is called the maximum torque per volt (MTPV). The curve BC in Figure 2 represents the MTPV curve. The working points in the current coordinate dq are determined through (12) based on [29].

$$i_d = \frac{-\lambda_{pm}}{L_d} - \Delta id$$

$$i_q = \frac{\sqrt{V_{s,max}^2 / \omega_e^2 - (L_d . \Delta id)^2}}{L_q}$$

$$(12)$$

$$\Delta id = \frac{-\lambda_{pm}.L_q + \sqrt{(\lambda_{pm}.L_q)^2 + 8\left(L_d - L_q\right)^2 V_{s,max}^2 / \omega_e^2}}{4 L_d \left(L_q - L_d\right)}$$

$$(13)$$

where Δid is determined based on (13).

3. PROPOSED HYBRID SPEED CONTROL IN FLUX-WEAKENING AREA

3.1. Control principle of VCC and FVC in the FW region

The control principle of VCC and FVC in the FW region in the id-q plane is shown in detail, as shown in Figure 3. The VCC method changes the PMSM velocity by varying the current vector amplitude. Assume the motor is operating at the work point h_1. When accelerating or decelerating, the working point shifts to point h_3 or h_2 shown in Figure 3(a). At this time, the change in rotor speed will take place more slowly and cause the working point to leap out of the voltage limit ellipse. It leads to instability in PMSM speed control. Thus, the VCC control method is ineffective in changing motor speed when working in the FW region. However, when the operating point is at the boundary of the FW region (MTPA, MC, and MTPV curve), the VCC shows the ability to minimize over-current during control. When it comes to accelerating with the maximum possible torque ($i_s = i_{max}$), VCC is a suitable choice.

The FVC method changes the PMSM speed by moving along the voltage limit curve. It is easy to see that the torque at the point h_5 is greater than that of h_4, as shown in Figure 3(b). The flux angle will be increasing To increase the torque and lead to an increase the speed. Notice that increasing the flux angle does not lead to over the back EMF when both operating points stay at the voltage limit ellipse. It shows that if we want to change the velocity of PMSM while working in the FW region, this method will bring about a more stable effect. However, increasing the alpha causing the working point to exceed the current limiting circle, resulting in instability in the rotor speed control. Thus, the FVC control method is highly effective when the operating point is within the FW region with the reference current amplitude smaller than the maximum current amplitude. When increasing the torque causes the operating point to go out of the current limiting curve, the VCC method gives better control results.
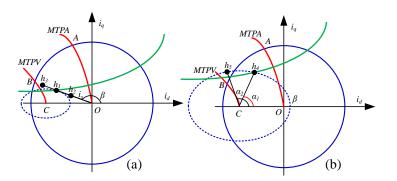

Figure 3. Principle of VCC and FVC methods on the id-q plane

3.2. Combined flux-weakening velocity regulation of VCC and FVC control

In this paper, a hybrid method is proposed to overcome the shortcomings and take advantage of VCC and FVC. The appropriate PMSM velocity control method was selected when Comparing the desired current vector amplitude value with the rated current. When accelerating with the rated current amplitude, the VCC method is used to minimize over-current. When the current vector magnitude is lower than its nominal value, the FVC method ensures that the limit voltage condition is satisfied. Figure 4 illustrates the principle of proposed switching regulation technique.
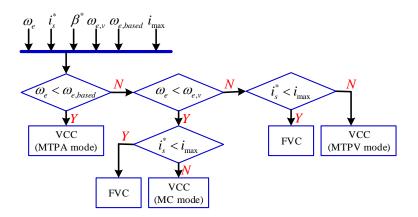

Figure 4. Switching rule in the proposed control method

4. RESULTS AND ANALYSIS
4.1. PMSM speed regulation

IPMSM velocity controller simulation model performed by Matlab/Simulink software was performed to evaluate the IPMSM velocity control method's obtained efficiency in the FW region. Table 2 is given The PMSM motor parameters, which follow data from Fadel in [29]. The model consists of two main blocks, the IPMSM motor block, and the control block, as shown in Figure 5. The model is built with three

different control methods: VCC, FVC, and the proposed hybrid control method, to have sufficient data to estimate the efficiency of the novel hybrid control technique. The results obtained in the simulation are detailed in the following sections.

Table 2. IPMSM coefficients

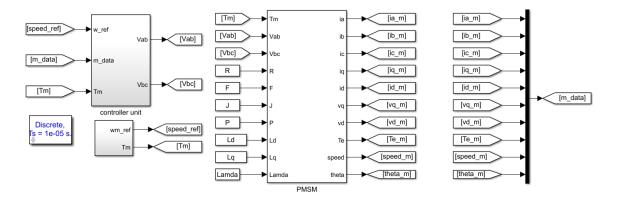| Coefficient	Rated magnitude	Unit
R	0.97	Ω
Ld	4.73	mH
Lq	5.77	mH
λpm	0.0345	Wb
P	5	
Imax	8	A
Vdc	200	V

Figure 5. IPMSM speed control diagram

4.2. Results of PMSM combined regulation technique

The reference velocity and loaded moment are proposed to estimate the efficiency of IPMSM velocity control methods in the FW region in different operating controls, as shown in Figure 6. The proposed criteria include acceleration time, overshoot speed during variable speed, ability to respond to variable rotor speed with varying load torque, and the PMSM current and electric torque disturbance to assess the proposed method's efficacy. The rotor speed shall be capable of withstanding the reference velocity applied to the controller under different torque conditions, as shown in Figure 6.
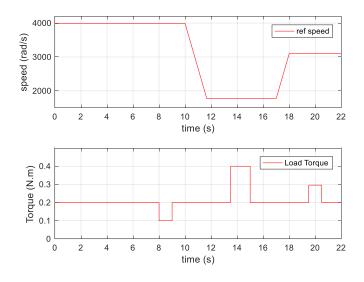

Figure 6. Reference PMSM rotor speed and load torque

Figure 7(a) shows the change of speed of IPMSM according to the reference velocity of different algorithms. Simulation results show that the rotor speed can follow the reference speed in all three control methods. However, the ability to follow the reference velocity of each technique is significantly different. The VCC method and the proposed method have faster response times than the magnetic direct calculation method. The reason is that fluctuation of the reference working point in the DCC method cannot give the maximum torque value during acceleration due to violation of the current limit line.

Figure 7(b) shows the simulation results of the PMSM speed in response to the change in load torque when the motor speed reaches the reference speed. At time t=8 s, a decrease in the load torque causes the overshoot speed. With different algorithms, this change is further. The proposed method has a small overshoot, while the VCC algorithm has the highest overshoot. Similarly, at t=9 s, the load torque increases, the imbalance between the load torque and the electromagnetic torque decreases the motor speed. In response to this reduction, the proposed method has the least reduction in rotor speed. Thus, the proposed method has a better answer to the change in load torque.

Figure 7(c) shows the response of the algorithms to the change in reference velocity. Through the results, it can be seen that the VCC method responds faster than the other methods. However, this method still has high overshoots and takes a long time to stabilize. On the contrary, the proposed method is not as fast as VCC but has fast stability according to the reference speed and almost prevents the overshoot when accelerating. Thus, the results in Figure 7(c) show that the ability to stick firmly according to the proposed hybrid control's PMSM reference speed.
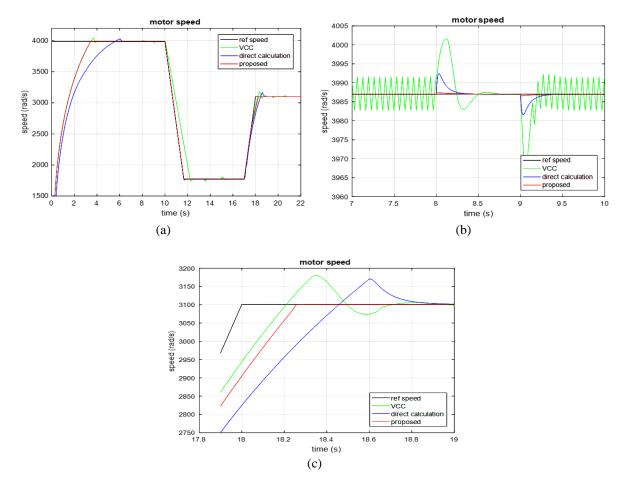

(a)

(b)

(c)

Figure 7. IPMSM speed during simulation

Figure 8(a) shows the results of the electromagnetic moment in the PMSM generated during operation by various control methods. From the picture, we can immediately see that the VCC method has the most extensive electromagnetic moment disturbance in the FW region. The DCC method has fluctuations during the start-up process when it passes through the MC region. The cause of the turbulence of this method is a violation of the current limit circle.

Figure 8(b) is the enlargement of Figure 8(a). It indicates the change in the electromagnetic torque with the growth of the load torque. Notice that when the load torque changes, the electromagnetic torque also changes. During the stabilization process, the electromagnetic torque still fluctuates wildly due to voltage violations in the VCC method FW region. The other two ways do not oscillate because they do not violate the voltage in the FW region.

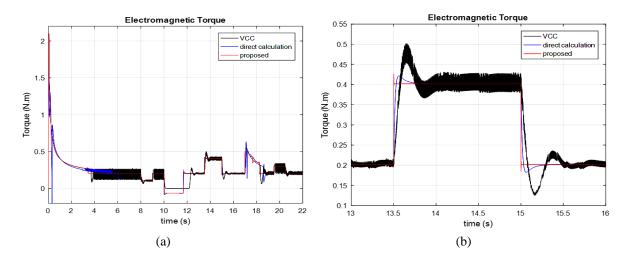| (a)   (b) |

Figure 8. Electromagnetic torque of IPMSM during simulation

Figure 9(a) shows simulation results of d- and q-axis current. It can be seen from the figure that the currents via the VCC method still fluctuate when entering the FW region. The reason is that this method is that the reference voltage is always fluctuating when operating at the voltage limit circle. The other two ways do not suffer from this phenomenon due to flux as a control variable, so no reference voltage violation occurs. Also, due to the control axis change measure's use, the current response will be faster, as shown in Figure 9(b). Based on the obtained simulation results, it is clear to see that the new PMSM combined regulation technique is highly effective in controlling the PMSM motor in FW when the comparison criteria give better results than the methods used as reference are VCC and DCC.
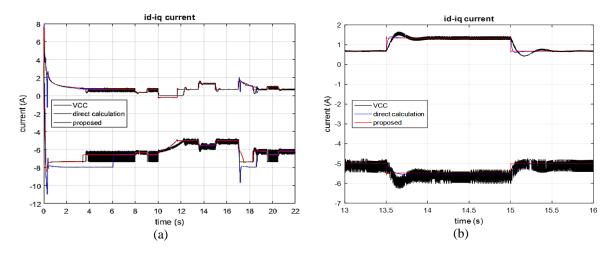

| (a)   (b) |

Figure 9. *dq*-axis current of IPMSM during simulation

5.   CONCLUSION

This study introduces a hybrid IPMSM velocity control technique between two typical control methods, FVC and VCC, operated on FW area. The proposed technique's selection combine these two methods is made by mapping the reference stator current its rated value. The principle of switching between

the two modes is simple and requires no additional hardware structure. Compared with the simulation results of the two classic methods, VCC and DCC, the proposed hybrid velocity control algorithm provide a new approach with high efficiency in improving control quality and improving speed. Stabilizes and reduces electromagnetic current and torque. With the hybrid method between the two methods VCC and FVC, newly proposed PI closed-loop controllers are used, making it challenging to experimentally adjust controllers' parameters. More research is needed to fix this problem in the coming research.

REFERENCES

[1] F. Leach, G. Kalghatgi, R. Stone, and P. Miles, "The scope for improving the efficiency and environmental impact of internal combustion engines," *Transp. Eng.*, vol. 1, 2020, doi: 10.1016/j.treng.2020.100005.

[2] T. Deng, Z. Su, J. Li, P. Tang, X. Chen, and P. Liu, "Advanced Angle Field Weakening Control Strategy of Permanent Magnet Synchronous Motor," *IEEE Trans. Veh. Technol.*, vol. 68, no. 4, pp. 3424–3435, Apr. 2019, doi: 10.1109/TVT.2019.2901275.

[3] F. Amin, E. Bin Sulaiman, W. M. Utomo, H. A. Soomro, M. Jenal, and R. Kumar, "Modelling and Simulation of Field Oriented Control based Permanent Magnet Synchronous Motor Drive System," *Indonesian Journal of Electrical Engineering and Computer Science (IJEECS)*, vol. 6, no. 2, pp. 387–395, May 2017, doi: 10.11591/ijeecs.v6.i2.pp387-395.

[4] A. A. Abd Samat, M. Zainal, L. Ismail, W. S. Saidon, and A. I. Tajudin, "Current PI-Gain Determination for Permanent Magnet Synchronous Motor by using Particle Swarm Optimization," *Indonesian Journal of Electrical Engineering and Computer Science (IJEECS),* vol. 6, no. 2, pp. 412–421, May 2017, doi: 10.11591/ijeecs.v6.i2.pp412-421.

[5] J. M. Lazi, Z. Ibrahim, M. Talib, A. Alias, A. Nur, and M. Azri, "Speed and position estimator of for sensorless PMSM drives using adaptive controller," *International Journal of Power Electronics and Drive Systems (IJPEDS),* vol. 10, no. 1, pp. 128–136, 2019, doi: 10.11591/ijpeds.v10.i1.pp128-136.

[6] L. M'hamed, A. Roufaida, A. A. M. Nawa, and A. ameur mezyane Nawal, "Sensorless control of PMSM with fuzzy model reference adaptive system," *International Journal of Power Electronics and Drive Systems (IJPEDS),* vol. 10, no. 4, pp. 1772–1780, 2019, doi: 10.11591/ijpeds.v10.i4.pp1772-1780.

[7] O. M. Arafa, S. A. Wahsh, M. Badr, and A. Yassin, "Grey wolf optimizer algorithm based real time implementation of PIDDTC and FDTC of PMSM," *International Journal of Power Electronics and Drive Systems (IJPEDS)*, vol. 11, no. 3, pp. 1640−1652, Sep. 2020, doi: 10.11591/ijpeds.v11.i3.pp1640-1652.

[8] A. Idir, A. Ahriche, K. Khettab, Y. Bensafia, and M. Kidouche, "Real time simulation of sensorless control based on back-EMF of PMSM on RT-Lab/ARTEMIS real-time digital simulator," *Int. J. Adv. Appl. Sci.*, vol. 8, no. 4, pp. 269–278, Dec. 2019, doi: 10.11591/ijaas.v8.i4.pp269-278.

[9] J. Dong, Y. Huang, L. Jin, and H. Lin, "Comparative Study of Surface-Mounted and Interior Permanent-Magnet Motors for High-Speed Applications," *IEEE Trans. Appl. Supercond.*, vol. 26, no. 4, pp. 1–4, Jun. 2016, doi: 10.1109/TASC.2016.2514342.

[10] T. M. Jahns, "Flux-Weakening Regime Operation of an Interior Permanent-Magnet Synchronous Motor Drive," *IEEE Trans. Ind. Appl.*, vol. IA-23, no. 4, pp. 681–689, Jul. 1987, doi: 10.1109/TIA.1987.4504966.

[11] X. Liu, H. Chen, J. Zhao, and A. Belahcen, "Research on the Performances and Parameters of Interior PMSM Used for Electric Vehicles," *IEEE Trans. Ind. Electron.*, vol. 63, no. 6, pp. 3533–3545, Jun. 2016, doi: 10.1109/TIE.2016.2524415.

[12] F. Chai, K. Zhao, Z. Li, and L. Gan, "Flux Weakening Performance of Permanent Magnet Synchronous Motor With a Conical Rotor," *IEEE Trans. Magn.*, vol. 53, no. 11, pp. 1–6, Nov. 2017, doi: 10.1109/TMAG.2017.2708139.

[13] Z. Zhang, C. Wang, M. Zhou, and X. You, "Flux-Weakening in PMSM Drives: Analysis of Voltage Angle Control and the Single Current Controller Design," *IEEE J. Emerg. Sel. Top. Power Electron.*, vol. 7, no. 1, pp. 437–445, Mar. 2019, doi: 10.1109/JESTPE.2018.2837668.

[14] R. S. Akhil, V. P. Mini, N. Mayadevi, and R. Harikumar, "Modified Flux-Weakening Control for Electric Vehicle with PMSM Drive," *IFAC-PapersOnLine*, vol. 53, no. 1, pp. 325–331, 2020, doi: 10.1016/j.ifacol.2020.06.055.

[15] Y. Chen *et al*., "Improved Flux-Weakening Control of IPMSMs Based on Torque Feedforward Technique," *IEEE Trans. Power Electron.*, vol. 33, no. 12, pp. 10970–10978, Dec. 2018, doi: 10.1109/TPEL.2018.2810862.

[16] N. Li and X. Cao, "High Speed PMSM Anti-saturation Regulation Method Based on Hybrid Flux Weakening Technology," *E3S Web Conf.*, Dec. 2019, vol. 136, Art. No. 02011, doi: 10.1051/e3sconf/201913602011.

[17] W. Zhang, F. Xiao, J. Liu, Z. Mai, and C. Li, "Optimization of maximum torque output in the wide speed range of a PMSM traction control system," *J. Power Electron.*, vol. 20, no. 1, pp. 152–162, Jan. 2020, doi: 10.1007/s43236-019-00008-3.

[18] C. Wang and Z. Q. Zhu, "Fuzzy Logic Speed Control of Permanent Magnet Synchronous Machine and Feedback Voltage Ripple Reduction in Flux-Weakening Operation Region," *IEEE Trans. Ind. Appl.*, vol. 56, no. 2, pp. 1505–1517, 2020, doi: 10.1109/TIA.2020.2967673.

[19] K. Chen, Y. Sun, and B. Liu, "Interior Permanent Magnet Synchronous Motor Linear Field-Weakening Control," *IEEE Trans. Energy Convers.*, vol. 31, no. 1, pp. 159–164, Mar. 2016, doi: 10.1109/TEC.2015.2478917.

[20] C. Miguel-Espinar, D. Heredero-Peris, G. Gross, M. Llonch-Masachs, and D. Montesinos i Miracle, "Maximum Torque per Voltage Flux-Weakening strategy with speed limiter for PMSM drives," *IEEE Trans. Ind. Electron.*, 2020, doi: 10.1109/TIE.2020.3020029.

[21] V. Manzolini, D. Da Ru, and S. Bolognani, "An Effective Flux Weakening Control of a SyRM Drive Including MTPV Operation," *IEEE Trans. Ind. Appl.*, vol. 55, no. 3, pp. 2700–2709, May 2019, doi: 10.1109/TIA.2018.2886328.

[22] Y. Zbede and J. Apsley, "Field weakening control of a PM vehicle drive," *J. Eng.*, vol. 2019, no. 17, pp. 3510–3515, Jun. 2019, doi: 10.1049/joe.2018.5347.

[23] L. Tang, L. Zhong, M. F. Rahman, and Y. Hu, "A Novel Direct Torque Controlled Interior Permanent Magnet Synchronous Machine Drive With Low Ripple in Flux and Torque and Fixed Switching Frequency," *IEEE Trans. Power Electron.*, vol. 19, no. 2, pp. 346–354, Mar. 2004, doi: 10.1109/TPEL.2003.823170.

[24] G. Pellegrino, E. Armando, and P. Guglielmi, "Direct Flux Field-Oriented Control of IPM Drives With Variable DC Link in the Field-Weakening Region," *IEEE Trans. Ind. Appl.*, vol. 45, no. 5, pp. 1619–1627, 2009, doi: 10.1109/TIA.2009.2027167.

[25] A. Yousefi-Talouki, P. Pescetto, and G. Pellegrino, "Sensorless Direct Flux Vector Control of Synchronous Reluctance Motors Including Standstill, MTPA, and Flux Weakening," *IEEE Trans. Ind. Appl.*, vol. 53, no. 4, pp. 3598–3608, Jul. 2017, doi: 10.1109/TIA.2017.2679689.

[26] S. Bolognani, S. Calligaro, R. Petrella, and F. Pogni, "Flux-weakening in IPM motor drives: Comparison of state-of-art algorithms and a novel proposal for controller design," *Proc. 2011 14th Eur. Conf. Power Electron. Appl. EPE 2011*, 2011.

[27] D. Hu, L. Zhu, and L. Xu, "Maximum Torque per Volt operation and stability improvement of PMSM in deep flux-weakening Region," in *2012 IEEE Energy Conversion Congress and Exposition (ECCE)*, Sep. 2012, pp. 1233–1237, doi: 10.1109/ECCE.2012.6342675.

[28] N. Mohan and N. Mohan, "Advanced Electric Drives: Analysis, Control, and Modeling Using MATLAB/Simulink," Hoboken, NJ, USA, John Wiley & Sons, Inc., vol. 136, no. 1, 2014.

[29] L. Sepulchre, M. Fadel, M. Pietrzak-David, and G. Porte, "MTPV Flux-Weakening Strategy for PMSM High Speed Drive," *IEEE Trans. Ind. Appl.*, vol. 54, no. 6, pp. 6081–6089, Nov. 2018, doi: 10.1109/TIA.2018.2856841.

BIOGRAPHIES OF AUTHORS

Pham Quoc Khanh received the BS and the M.Sc. degrees in the Department of Electrical and Electronics Engineering from HCM City University of Technology and Education in 2009 and 2013. He is currently a Lecturer in the Faculty of Electricity Technology (FEE), Industrial University of Ho Chi Minh City, Vietnam. His current research interests include intelligent control, renewable energy, modeling and identification of nonlinear dynamic systems, and the power network's faulty location.

Ho Pham Huy Anh received the B.S. and the M.Sc. degrees in the Department of Electrical and Electronics Engineering from HCM City University of Technology (HCMUT), VNU-HCM in 1987 and in 1993, respectively. He received the Ph.D. degree from University of Ulsan, Korea in 2008. He is currently an Advanced Lecturer in the Faculty of Electrical and Electronics (FEEE), HCM City University of Technology, VNU-HCM, HCM City, Viet Nam. Up to now, he authored and co-authored 4 books and published over 140 papers on national and international journals and conference proceedings. His current research interests include intelligent control, robotics, novel energy applications, modeling and identification of nonlinear dynamic system, soft-computing.